Polarization interaction of spatial solitons in optical planar waveguides

A. D. Boardman,[1] K. Xie,[1] and A. A. Zharov[2]
[1]*Joule Laboratory, Department of Physics, University of Salford, Salford, M5 4WT, United Kingdom*
[2]*Laboratory of Solid State Spectroscopy, Institute of Applied Physics, Russian Academy of Sciences, Nizhnii, Novgorod, Russia*
(Received 31 May 1994)

Polarization-coupled spatial solitons in optical planar waveguides are investigated, using Whitham's average variational principle to cast the problem into a set of ordinary differential equations. The main problem addressed is the stability of the dynamics and the mathematical results derived are compared with linear stability theory. Analytical forms for the stability edges are given together with numerical work that confirms that the true soliton dynamics agree with the mathematical analysis.

PACS number(s): 42.65.−k, 42.50.Rh

I. INTRODUCTION

Much has been written about temporal soliton coupling [1–10] using various forms of coupled Schrödinger equations [1] and widely differing methods of solution [4–6,8–10]. The latter ranges from being almost entirely mathematical, through mixed approaches, based upon linear stability analysis, to entirely variational. In a rather elegant paper, Wright, Stegeman, and Wabnitz [4] used a linear stability analysis, backed up by some numerical experiments. In particular, they set up a model to study the coupling between two polarized modes in an optical fiber or those in a directional coupler. The linear stability analysis enabled them to predict the eventual decay of solitary waves into nonstationary states and forms of symmetry breaking. With respect to the latter, they classified the instabilities that ensue into (a) asymmetric (energy exchange between the two modes) and (b) symmetric (no energy exchange). Wright, Stegeman, and Wabnitz [4] also pointed out that other instabilities could exist and, interestingly enough, that their numerical work uncovered instabilities that were not predicted by their linear analysis.

Spatial solitons are beams of electromagnetic energy that rely upon balancing *diffraction* and *nonlinearity* to retain their shape [9,11–17]. In contrast, temporal solitons [1] are pulses that rely upon balancing phase changes across their width, which arise from material dispersion and nonlinearity. A light beam, even in a vacuum, will spread out as a result of diffraction, but a pulse requires a dispersive medium in order to suffer any spreading. Hence group velocity plays an important role in temporal soliton interactions, but does not feature in spatial soliton interactions [16]. Indeed group-velocity matching is required for the temporal case, but plays no role in spatial soliton interactions. As a consequence, interacting beams can be set at any angle to each other, even in an isotropic medium. The replacement of group-velocity dispersion by diffraction, in the case of spatial solitons, means therefore that superimposed beams, even with different wavelengths, can interact over large propagation lengths [16]. Diffraction is dependent on wavelengths, so some interactions for temporal solitons, which pair bright and dark solitons, have no spatial analog [16].

Novel soliton states and bifurcation phenomena in nonlinear optical waveguide couplers have been predicted recently on the basis of a limited mathematical, linear, stability analysis. It was shown, within this model [5], that new states appear at a point of bifurcation in the energy dispersion diagram. It is interesting that this linear stability analysis appears to show that the reason for the symmetry breaking predicted by Wright, Stegeman, and Wabnitz is the appearance of these new soliton states. Once this is established, then further infra-structure is identifiable concerning states, with energies above or below the bifurcation point being unstable or stable [5].

The validity of linear stability analysis as a means of studying the modulation of a continuous wave (cw) is widely accepted [1,2] and has been verified in many theoretical investigations [1,2]. It is, however, a more questionable technique for analyzing soliton phenomena. The problem is that the method, as deployed in the current literature, assumes that the *shape* of the perturbation (noise) remains constant during its evolution. Only the amplitude changes and, in the case of cws, such "noise" is assumed to be harmonic (sin or cos) in form, with the frequency of the disturbance (perturbation) being a free (disposable) parameter. This assumption is valid because, within a linear framework, any form of noise can be Fourier analyzed into a set of harmonic waves, with different frequencies. For solitons, however, because of the transverse shape change in the soliton itself, the noise treatable by linear instability analysis has been, of mathematical necessity, limited to only a few transverse shapes, which do not form a complete set. In addition, the noise changes shape during the evolving interaction with a strong soliton signal, indicating that the transverse and longitudinal variables cannot be separated.

The problem to be addressed here is described by coupled nonlinear Schrödinger equations. As will be shown later on, the length scale over which spatial solitons develop and interact is rather short compared to the temporal case. It is important, therefore, to retain all the nonlinear and linear coupling terms appropriate to this scale rather than prematurely removing some of them on the grounds that they average out to zero during the evo-

lution or interaction. It is recognized that coupled nonlinear Schrödinger equations, in dimensionless form, have a generic appearance and specialized solutions of them have been targeted on temporal solitons. Some cases exist in the literature [18–22], but, for applications to spatial solitons, suffer from some of the limitations outlined above.

The coupled nonlinear Schrödinger equations to be developed here have solutions yielding soliton dynamics that are coupled through two parameters which, at this stage, will be called ν (linear coupling) and μ (nonlinear coupling). For the three common nonlinear mechanisms, namely, thermal, electronic distortion, and molecular orientation, μ is 1, 2, and ∞, respectively, as will be demonstrated later on. Any restriction on the value of μ, especially confinement to nonphysical or quasi-physical values, is not a welcome aspect of any stability theory. Unfortunately linear stability theory does just this and restricts [4] μ to be $\mu<3$ for asymmetric perturbations and to be $\mu<1$ for symmetric perturbations. Hence the kind of linear analysis reported in the literature can only be used in the thermal and electronic cases for asymmetric perturbations, while the analysis of symmetric perturbations hardly applies to any of these nonlinear mechanisms [5]. Indeed, even thermal nonlinearity lies on the very edge ($\mu=1$) of the domain of applicability.

The study of soliton dynamics can be based upon variational theory [7–10,18–22]. Analytical progress rests upon the adoption of an average variational method, widely known as Whitham's method [23]. It centers upon the use of an average Lagrangian density and the inevitable introduction of trial functions. Detailed justification of the variational method has been given, most eloquently, by Whitham himself [23] and has been rather elegantly applied, mainly by Anderson and Lisak [10]. It has been used very effectively by Ueda and Kath [8] and Paré and Florjanczyk [6] to study coupled solitons. As Whitham points out [23], the method permits the generation of quite general results and is well able to deal with stability questions. Naturally, the accuracy of any description of spatial soliton beam dynamics will depend upon the choice of trial function.

Numerical simulations give the true beam dynamics and a mathematical description, proceeding via a variational method, and very general trial functions can be benchmarked safely by comparing the mathematical conclusions to the numbers generated. Paré and Florjanczyk studied the soliton dynamics [6] in all-optical couplers by a variational method that gives the stability edge for $\mu=0$ and an asymmetric perturbation. Even though their model fails for symmetric perturbations, it does show a possible way forward. This paper, therefore, also rests its stability analysis upon the average variational principle. Rather general trial functions are used, including a local phase change across the beam (spatial frequency chirp), to produce some new mathematical results. The trial functions used lead to certain stability conclusions that are checked by generating the true soliton dynamics numerically.

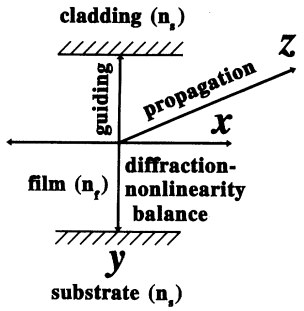

FIG. 1. Schematic illustration of spatial soliton in a slab waveguide.

II. COUPLED EQUATIONS

A weakly guided ($E_z\simeq 0$), weakly nonlinear TE, or TM, wave carries an electric field whose Fourier amplitude E_j satisfies the following equation:

$$\nabla^2 E_j+\frac{\omega^2}{c^2}n^2E_j+\mu_0\omega^2P_j^{\mathrm{NL}}=0\ . \tag{1}$$

It is presumed that the waves propagate in the planar optical waveguide shown in Fig. 1. ω is the angular frequency, c is the velocity of light in a vacuum, n is the linear refractive index of the waveguide material, μ_0 is the permeability of free space, $j=x$ for a TE wave, $j=y$ for a TM wave, and P_j^{NL} are the nonlinear polarizations. The expressions for P_j^{NL} are

$$\begin{aligned}P_x^{\mathrm{NL}}&=\tfrac{3}{4}\epsilon_0[(\chi_{xyyx}+\chi_{xxyy})(|E_x|^2+|E_y|^2)E_x+\chi_{xyxy}(E_x^2+E_y^2)E_x^*]\\&=\tfrac{3}{4}\epsilon_0[(\chi_{xyyx}+\chi_{xyxy}+\chi_{xxyy})(|E_x|^2+|E_y|^2)E_x+\chi_{xyxy}(E_x^2E_x^*+E_y^2E_x^*-|E_x|^2E_x-|E_y|^2E_x)]\ ,\end{aligned} \tag{2}$$

where χ_{ijkl} is a fourth-rank tensor describing the third-order nonlinear susceptibility. Since $\chi_{xxxx}=\chi_{xyyx}+\chi_{xxyy}+\chi_{xyxy}$, P_x^{NL} reduces to [24,25]

$$\begin{aligned}P_x^{\mathrm{NL}}&=\tfrac{3}{4}\epsilon_0[(\chi_{xxxx}(|E_x|^2+|E_y|^2)E_x\\&\quad+\chi_{xyxy}(E_yE_x^*-E_xE_y^*)E_y]\\&=\epsilon_0\alpha[(|E_x|^2+|E_y|^2)E_x+f(E_yE_x^*-E_y^*E_x)E_y]\ ,\end{aligned} \tag{3}$$

where $\alpha=\frac{3}{4}\chi_{xxxx}$ and $f=\frac{3}{4}(\chi_{xyxy}/\alpha)=\chi_{xyxy}/\chi_{xxxx}$. Similarly,

$$P_y^{\mathrm{NL}}=\epsilon_0\alpha[(|E_x|^2+|E_y|^2)E_y+f(E_y^*E_x-E_yE_x^*)E_x]\ . \tag{4}$$

Note that $f=3\chi_{yxyx}/4\alpha=3\chi_{xyxy}/4\alpha=0,\frac{1}{3},1$ for thermal, electronic distortion, or molecular orientational nonlinear mechanisms, respectively.

The substitution of Eqs. (3) and (4) into Eq. (1) yields

$$\nabla^2 E_j+\frac{\omega^2}{c^2}(n^2+\Delta n_j^2)E_j=0\ , \tag{5}$$

where

$$\Delta n_j^2=\alpha\left[(|E_j|^2+|E_k|^2)+f\left[\frac{E_j^*}{E_j}E_k^2-|E_k|^2\right]\right]\ ,$$

$$k,j=x,y,\ j\neq k\ .$$

The transverse dependence can be factored out by using the separable solution

$$E_j(x,y,z)=\Gamma A_j(y)B_j(x,z)\exp\left[i\frac{\omega}{c}\beta z\right]\ , \tag{6}$$

where $A_j(y)$ is the *linear* modal field, $B_j(x,z)$ is a slowly varying amplitude envelope, $\beta=(\beta_x+\beta_y)/2$, $(\omega/c)\beta_{x,y}$ are *unperturbed* wave numbers, and $\Gamma^2=1/\int A_x^2dy=1/\int A_y^2dy$ (normalization factors).

Substitution of Eq. (6) into Eq. (5) leads to

$$i2\frac{\omega}{c}\beta\frac{\partial B_j}{\partial z}+\frac{\partial^2 B_j}{\partial x^2}+\frac{\omega^2}{c^2}(\beta_j'^2-\beta_j^2\pm 2\nu)B_j=0\ , \tag{7}$$

where $2\nu=\beta(\beta_x-\beta_y)$ and β_j' is determined from the modal equation

$$\frac{\partial^2 A_i}{\partial y^2}+\frac{\omega^2}{c^2}(n^2+\Delta n_j^2-\beta_j'^2)A_j=0\ ,$$

which immediately gives

$$\beta_j'^2-\beta_j^2=\frac{\int\Delta n_j^2|A_j|^2dy}{\int|A_j|^2dy}=\alpha'\left[|B_j|^2+|B_k|^2+f\left[\frac{B_j^*}{B_j}B_k^2-|B_k|^2\right]\right]\ , \tag{8}$$

where

$$\alpha'=\alpha\frac{\int|A_j|^4dy}{\left[\int|A_j|^2dy\right]^2}=\alpha\frac{\int|A_j|^2|A_k|^2dy}{\left[\int|A_j|^2dy\right]^2}\ .$$

After substituting Eq. (8) into Eq. (7), and after making the transformations

$$\frac{\omega}{c}x\rightarrow x,\quad \frac{\omega}{c}z\rightarrow 2\beta z,\quad \left[\frac{\alpha'}{2}\right]^{1/2}B_j\rightarrow\psi_j\ ,$$

the following coupled equations are obtained:

$$i\frac{\partial\psi_x}{\partial z}+\frac{\partial^2\psi_x}{\partial x^2}+2\nu\psi_x+2(|\psi_x|^2+|\psi_y|^2)\psi_x+2f(\psi_x^*\psi_y-\psi_x\psi_y^*)\psi_y=0\ , \tag{9a}$$

$$i\frac{\partial\psi_y}{\partial z}+\frac{\partial^2\psi_y}{\partial x^2}-2\nu\psi_y+2(|\psi_x|^2+|\psi_y|^2)\psi_y+2f(\psi_y^*\psi_x-\psi_y\psi_x^*)\psi_x=0\ . \tag{9b}$$

Note that the terms $\psi_x^*\psi_y^*$ and $\psi_y^*\psi_x^2$ must be retained for spatial solitons because the physical diffraction scale is such that they do not average to zero. For intended applications to temporal solitons, however, these terms are always omitted [8,10,18,21]. If $\psi_x^*\psi_y^2$ and $\psi_y^*\psi_x^2$ are neglected, Eqs. (9a) and (9b) immediately return to (3a) and (3b) of Ueda and Kath [8] or the equations used by Kaup, Malomed, and Tasgal [18]. Upon neglect of the $\psi_x^*\psi_y^2$ and $\psi_y^*\psi_x^2$, Eqs. (9a) and (9b) still have $2\nu\psi_x$ and $-2\nu\psi_y$. This is not a problem, however, since the latter terms can be easily removed by the transformations $\psi_x\rightarrow\psi_x e^{2i\nu z}$ and $\psi_y\rightarrow\psi_y e^{-2i\nu z}$.

Equation (9) can be used to describe the evolution of the two orthogonally polarized components of a electromagnetic wave field in a planar waveguide. If only one field component is launched, a scalar solution of Eqs. (9) is generated. The alternatives are

$$\psi_x=\rho\,\mathrm{sech}(\rho x)\exp[i(\rho^2+2\nu)z],\quad \psi_y=0$$

for the TE soliton , (10a)

$$\psi_x=0,\quad \psi_y=-i\rho\,\mathrm{sech}(\rho x)\exp[i(\rho^2-2\nu)z]$$

for the TM soliton (10b)

III. VARIATIONAL MODEL

The Whitham variational approach to problems of this kind is well described in an earlier paper [9], so only the briefest background details will be given here. Before even this is done, however, it is convenient to transform the equations to a rotating polarization frame of reference. In fact, right and left elliptically polarized field amplitudes can be defined as

$$\psi_1=\frac{\sqrt{1-f}}{\sqrt{2}}(\psi_x+i\psi_y),\quad \psi_2=\frac{\sqrt{1-f}}{\sqrt{2}}(\psi_x-i\psi_y)\ . \tag{11}$$

Hence, if a new constant $\mu=(1+f)/(1-f)$ is introduced, the coupled Schrödinger equations become

$$\begin{aligned} &i\frac{\partial\psi_1}{\partial z}+\frac{\partial^2\psi_1}{\partial x^2}+2\nu\psi_2+2(|\psi_1|^2+\mu|\psi_2|^2)\psi_1=0\ ,\\ &i\frac{\partial\psi_2}{\partial z}+\frac{\partial 2\psi_2}{\partial x^2}+2\nu\psi_1+2(|\psi_2|^2+\mu|\psi_1|^2)\psi_2=0\ . \end{aligned} \tag{12}$$

These are now in a form recognizable in the literature. In this new frame, the scalar soliton solutions are

$$\psi_1=\pm\psi_2=\frac{\rho}{\sqrt{1+\mu}}\mathrm{sech}(\rho x)\exp[i(\rho^2\pm 2\nu)z]\ . \tag{13}$$

The Lagrangian density [26] that yields Eqs. (12) is

$$L=\sum_{j=1}^{2}\left\{\frac{i}{2}\left[\psi_j^*\frac{\partial\psi_j}{\partial z}-\frac{\partial\psi_j^*}{\partial z}\psi_j\right]-\left|\frac{\partial\psi_j}{\partial x}\right|^2+|\psi_j|^4\right\}+2\nu(\psi_1^*\psi_2+\psi_1\psi_2^*)+2\mu|\psi_1|^2|\psi_2|^2 \tag{14}$$

and the general (yet still chirpless) trial function that will be used is

$$\psi_j=\eta_j \operatorname{sech}[\rho_j(x-x_j)]\exp\left[i\frac{\xi_j}{2}(x-x_j)+i\theta_j\right] . \quad (15)$$

Here the complete set of variational parameters $(\eta_j\rho_j\xi_j x_j\theta_j)$ varies as the propagation proceeds. They are defined as the beam amplitudes η_j, the widths of the beams $1/\rho_j$, the angles that the beams make to the z axis ξ_j, the positions of the beam centers x_j, and θ_j the phases. The average Lagrangian is achieved by an integration over x, which is the transverse direction that lies in the plane of the waveguide. The details of the averaged Lagrangian and the conservation laws that flow from it can easily be obtained from the earlier study [9].

If

$$\frac{\eta_2^2}{\rho_2}-\frac{\eta_1^2}{\rho_1}=2N, \quad \frac{\eta_2^2}{\rho_2}x_2-\frac{\eta_1^2}{\rho_1}x_1=2M\Delta ,$$
$$\frac{\eta_2^2}{\rho_2}\xi_2-\frac{\eta_1^2}{\rho_1}\xi_1=2M\xi, \quad \theta=\theta_2-\theta_1 , \quad (16)$$

where

$$2M=\frac{\eta_1^2}{\rho_1}+\frac{\eta_2^2}{\rho_2} \quad (17)$$

is a constant which represents the total energy of the coupled soliton, then

$$\frac{dN}{dz}=2\ \nu\sqrt{\rho_1\rho_2(M^2-N^2)}\int \operatorname{sech}\left[\rho_1\left[x+\frac{M\Delta}{M-N}\right]\right]\operatorname{sech}\left[\rho_2\left[x-\frac{M\Delta}{M+N}\right]\right]$$
$$\times\sin\left[\frac{M^2\xi}{M^2-N^2}x+\frac{2M^3N\Delta\xi}{(M^2-N^2)^2}+\theta\right]dx , \quad (18)$$

$$M\frac{d\Delta}{dz}=M\xi+2\nu\sqrt{\rho_1\rho_2(M^2-N^2)}\int x\operatorname{sech}\left[\rho_1\left[x+\frac{M\Delta}{M-N}\right]\right]\operatorname{sech}\left[\rho_2\left[x-\frac{M\Delta}{M+N}\right]\right]$$
$$\times\sin\left[\frac{M^2\xi}{M^2-N^2}x+\frac{2M^3N\Delta\xi}{(M^2-N^2)^2}+\theta\right]dx , \quad (19)$$

$$M\frac{d\xi}{dz}=2\nu\sqrt{\rho_1\rho_2(M^2-N^2)}\int \operatorname{sech}\left[\rho_1\left[x+\frac{M\Delta}{M-N}\right]\right]\operatorname{sech}\left[\rho_2\left[x-\frac{M\Delta}{M+N}\right]\right]$$
$$\times\left\{\rho_2\tanh\left[\rho_2\left[x-\frac{M\Delta}{M+N}\right]\right]-\rho_1\tanh\left[\rho_1\left[x+\frac{M\Delta}{M-N}\right]\right]\right\}$$
$$\times\cos\left[\frac{M^2\xi}{M^2-N^2}x+\frac{2M^3N\Delta\xi}{(M^2-N^2)^2}+\theta\right]dx$$
$$-2\nu\sqrt{\rho_1\rho_2(M^2-N^2)}\frac{MN\xi}{M^2-N^2}\int \operatorname{sech}\left[\rho_1\left[x+\frac{M\Delta}{M-N}\right]\right]\operatorname{sech}\left[\rho_2\left[x-\frac{M\Delta}{M+N}\right]\right]$$
$$\times\sin\left[\frac{M^2\xi}{M^2-N^2}x+\frac{2M^3N\Delta\xi}{(M^2-N^2)^2}+\theta\right]dx$$
$$+2\mu\rho_1\rho_2(M^2-N^2)\int \operatorname{sech}^2\left[\rho_1\left[x+\frac{M\Delta}{M-N}\right]\right]\operatorname{sech}^2\left[\rho_2\left[x-\frac{M\Delta}{M+N}\right]\right]$$
$$\times\left\{\rho_2\tanh\left[\rho_2\left[x-\frac{M\Delta}{M+N}\right]\right]-\rho_1\tanh\left[\rho_1\left[x+\frac{M\Delta}{M-N}\right]\right]\right\}dx . \quad (20)$$

Equations for $d\theta/dz$, ρ_1, and ρ_2 can also be derived with some effort, but in a straightforward way. They are rather bulky and will not be quoted here.

The system of equations involving dN/dz, $d\Delta/dz$, $d\xi/dz$, $d\theta/dz$, and $\rho_{1,2}$ has the stationary solution

$$\Delta=0, \quad N=0, \quad \xi=0, \quad \theta=\theta_0=0,\pm\pi, \quad \rho_1=\rho_2 \quad (21)$$

for which

$$\frac{dN}{dz}=0, \quad \frac{d\xi}{dz}=0, \quad \frac{d\Delta}{dz}=0, \quad \frac{d\theta}{dz}=0 .$$

It can be shown that Eq. (21) means Eq. (13), i.e.,

$$\rho_1=\rho_2=\rho=(1+\mu)M, \quad \eta_1=\eta_2=\eta=\frac{\rho}{\sqrt{1+\mu}}$$

and

$$\frac{d\theta_1}{dz}=\frac{d\theta_2}{dz}=\rho^2\pm 2\nu \ .$$

A stability analysis will now be undertaken.

IV. STABILITY ANALYSIS OF THE STATIONARY STATE

The stability analysis proceeds by introducing perturbations to N,Δ,ξ, and θ and then checking their evolution to see if they grow or decay. The stability analysis is simplified by the special nature of the coupled equations of dN/dz, $d\Delta/dz$, $d\xi/dz$, and $d\theta/dz$. Around the stationary state, (N,θ) and (ξ,Δ) evolve independently of each other. For example, a perturbation on N or θ will cause $dN/dz\neq 0$ and $d\theta/dz\neq 0$, but $\xi=0$, $\Delta=0$, $d\xi/dz=0$, and $d\Delta/dz=0$ are unchanged. This is because, from Eqs. (19) and (20), $d\xi/dz=d\Delta/dz=0$, once $\xi=\Delta=0$. On the other hand, $d\xi/dz=d\Delta/dz=0$ guarantees $\xi=\Delta=0$ for the next step in the propagation. For the same reason, a perturbation of Δ or ξ will cause $d\Delta/dz\neq 0$ and $d\xi/dz\neq 0$, but will not affect $\rho_1=\rho_2$, $N=0$, $\theta_0,\pm\pi$, and $dN/dz=d\theta/dz=0$. This property of the equations permits independent perturbation analysis of (N,θ) and (ξ,Δ). The final verdict concerning the stability of the physical system is arrived at after a linear summation of the results obtained from the two separate investigations.

A. Perturbation of Δ and ξ

This kind of perturbation changes the position of the beam center Δ and the beam propagation direction ξ. It also changes the beam width ρ_j. But, since the two solitons are symmetric, the relationship $\rho_1=\rho_2=\rho$ is always maintained in the system. The evolution equations for Δ, ξ, and ρ are

$$\frac{d\Delta}{dz}=\xi+2\nu\rho\int x\,\mathrm{sech}[\rho(x+\Delta)]\mathrm{sech}[\rho(x-\Delta)]\sin(\xi x)dx \ , \tag{22}$$

$$\frac{d\xi}{dz}=2\nu\rho^2\int \mathrm{sech}[\rho(x+\Delta)]\mathrm{sech}[\rho(x-\Delta)]\{\tanh[\rho(x-\Delta)]-\tanh[\rho(x+\Delta)]\}\cos(\xi x)dx$$
$$+2\mu\rho^3\int \mathrm{sech}^2[\rho(x+\Delta)]\mathrm{sech}^2[\rho(x-\Delta)]\{\tanh[\rho(x-\Delta)]-\tanh[\rho(x+\Delta)\}dx \ , \tag{23}$$

and

$$\tfrac{2}{3}(1-\rho)+\nu\int \mathrm{sech}[\rho(x+\Delta)]\mathrm{sech}\rho(x-\Delta)]\cos(\xi x)dx+\mu\rho\int \mathrm{sech}^2[\rho(x+\Delta)]\mathrm{sech}^2[\rho(x-\Delta)]dx$$
$$-\nu\rho\int \mathrm{sech}[\rho(x+\Delta)]\mathrm{sech}[\rho(x-\Delta)]\{(x-\Delta)\tanh[\rho(x-\Delta)]+(x+\Delta)\tanh[\rho(x+\Delta)]\}\cos(\xi x)dx$$
$$-\mu\rho^2\int \mathrm{sech}^2[\rho(x+\Delta)]\mathrm{sech}^2[\rho(x-\Delta)]\{(x-\Delta)\tanh[\rho(x-\Delta)]+(x+\Delta)\tanh[\rho(x+\Delta)]\}dx=0 \ , \tag{24}$$

where the variables have been normalized to

$$M^2z\to z, \quad Mx\to x, \quad \frac{\xi}{M}\to\xi, \quad M\Delta\to\Delta \ ,$$

$$\frac{M}{N}\to N, \quad \frac{\nu}{M^2}\cos\theta_0\to\nu, \quad \frac{\rho_j}{M}\to\rho \ .$$

Equations (22)–(24) reveal that the system has a constant of motion C, representing the Hamiltonian property of the system, which satisfies the equation

$$\tfrac{2}{3}\rho^2-\tfrac{4}{3}\rho+\tfrac{1}{2}\xi^2-2\nu\rho\int \mathrm{sech}[\rho(x+\Delta)]$$
$$\times\mathrm{sech}[\rho(x-\Delta)]\cos(\xi x)dx-\mu\rho^2$$
$$\times\int \mathrm{sech}^2[\rho(x+\Delta)]\mathrm{sech}^2[\rho(x-\Delta)]dx=C \ . \tag{25}$$

For the stability problem in hand, the initial conditions are $\rho|_{z=0}=1+\mu$, $\xi|_{z=0}=0$, and $\Delta|_{z=0}=0$, so that C is simply

$$C=-4\nu-\tfrac{2}{3}(1+\mu)^2 \ .$$

After performing the integrations, Eqs. (24) and (25) become

$$\tfrac{1}{3}(1-\rho)+\mu E-\frac{\nu}{\rho}F(G_2-G_3)+\mu 2\rho\Delta\frac{\partial E}{\partial(2\rho\Delta)}=0 \ , \tag{26}$$

$$\tfrac{2}{3}\rho^2-\tfrac{4}{3}\rho+\tfrac{1}{2}\xi^2-4\nu F-4\mu\rho E=-4\nu-\tfrac{2}{3}(1+\mu)^2 \ , \tag{27}$$

where

$$F=\frac{\pi\sin(\Delta\xi)}{\sinh(2\rho\Delta)\sinh\left[\dfrac{\pi\xi}{2\rho}\right]}, \quad G_3=\frac{\pi\xi}{2\rho}\coth\left[\frac{\pi\xi}{2\rho}\right] \ ,$$

$$G_1=\Delta\xi\cot(\Delta\xi), \quad G_2=2\rho\Delta\coth(2\rho\Delta) \ ,$$

$$E=\left[\frac{1}{\tanh^2(2\rho\Delta)}-1\right]\left[\frac{2\rho\Delta}{\tanh(2\rho\Delta)}-1\right] \ .$$

The evolution of the perturbations Δ, ρ, and ξ are controlled by the two algebraic equations (26) and (27). Initially $\Delta=0$, $\xi=0$, and $\rho=1+\mu$, but if the system is such that $\lim_{\Delta\to 0,\xi\to 0}d^2\xi^2/d\Delta^2<0$, ξ becomes pure imaginary for $\Delta\neq 0$. In a real system, of course, this can never occur, which means that Δ can *never* evolve away from $\Delta=0$. This system is considered, therefore, to be stable. On the other hand, a system for which

$\lim_{\Delta\to 0,\xi\to 0} d^2\xi^2/d\Delta^2 > 0$ is considered to be unstable.

Differentiating Eqs. (26) and (27) with respect to Δ leads to the following limiting values:

$$\lim_{\substack{\Delta\to 0\\ \xi\to 0}} \frac{d\rho}{d\Delta}=0, \quad \lim_{\substack{\Delta\to 0\\ \xi\to 0}} \frac{d\xi^2}{d\Delta}=0 , \tag{28}$$

$$\lim_{\substack{\Delta\to 0\\ \xi\to 0}} \left[\frac{d\xi}{d\Delta}\right]^2 = \lim_{\substack{\Delta\to 0\\ \xi\to 0}} \frac{1}{2}\frac{d^2\xi^2}{d\Delta^2} = -\frac{16}{3}\rho^2\left[\nu+\frac{4}{5}\mu\rho\right]\Big/\left[1+\frac{\pi^2}{3}\frac{\nu}{\rho^2}\right] , \tag{29}$$

where $\rho=1+\mu$. Instability is predicted, therefore, when

$$\frac{\frac{4}{5}\mu(1+\mu)+\nu}{1+\frac{\pi^2\nu}{3(1+\mu)^2}}<0 \tag{30}$$

and the two curves

$$\frac{4}{5}\mu(1+\mu)+\nu=0 , \tag{31}$$

$$1+\frac{\pi^2\nu}{3(1+\mu)^2}=0 , \tag{32}$$

plotted in Fig. 2, are the boundaries between the stable and unstable regions. Instability only occurs for $\nu<0$, that is, when two beams are opposite in phase ($\theta_0=\pm\pi$), i.e., the TE soliton is always stable. This analysis applies to several kinds of nonlinearity. In particular, for the molecular orientational nonlinear mechanism ($f=1$), $\mu\to\infty$, but the instability range can be transferred to ν-f space by the transformations $\nu\to\nu/M^2=[(1+\mu)^2/\rho^2]\nu$ and $\mu\to(1+f)/(1-f)$. In this case, Eqs. (31) and (32),

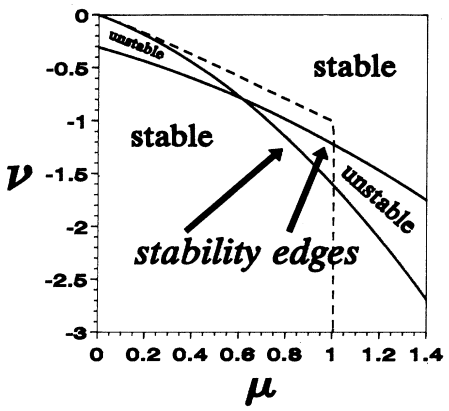

FIG. 2. (ν,μ) plane showing stable and unstable regions for the symmetric perturbations. Solid lines represent the Lagrangian theory and the dashed line denotes a linear stability analysis, for which the region contained by the dashed lines and the coordinate axes is unstable.

respectively, become $\nu/\rho^2=-\frac{2}{5}$ and $\nu/\rho^2=-3/\pi^2$, which indicates that TE solitons are always stable, while TM solitons are unstable when $3/\pi^2<|\nu/\rho^2|<\frac{2}{5}$ and stable everywhere else. This is confirmed by the numerical investigations reported in this paper.

A similar kind of perturbation has been studied by Wright, Stegeman, and Wabnitz using a linear instability analysis method, where it is classified as symmetric perturbation. Before the two results can be compared, a small improvement should be made to the previously reported linear instability analysis. In Ref. [4], the authors set $\lambda=\frac{1}{2}+\kappa$, where λ is the wave-number shift. In the notation of this paper, this corresponds to $\lambda\pm\nu=-\frac{1}{2}$, but this restriction is not necessary. Indeed, for any given value of λ, a stationary solution can be found in the form

$$\psi_1=\pm\psi_2=\left[\frac{-2\lambda\mp 2\nu}{1+\mu}\right]^{1/2} \times \operatorname{sech}(\sqrt{-2\lambda\mp\nu}\,x)\exp(-2i\lambda z)$$

and if ρ^2 is set to $-2\lambda\mp 2\nu$, then $\psi_1=\pm\psi_2=(\rho/\sqrt{1+\mu}\operatorname{sech}(\rho x)\exp[i(\rho^2\pm 2\nu)z]$.

After this minor modification, the linear stability analysis result is also plotted in Fig. 2 as a dashed line. In the range $0\le\mu<1$ (note that the linear result is not valid beyond $\mu=1$), the result given by the linear stability analysis is *qualitatively similar* to the curve given by Eq. (31). But the linear stability analysis does not generate the curve obtained from Eq. (32). This outcome is expected if it is recalled that Wright, Stegeman, and Wabnitz [4] use only certain instability edges in their analysis. These edges correspond to

$$\lim_{\substack{\Delta\to 0\\ \xi\to 0}} \left[\frac{d\xi}{d\Delta}\right]^2 = \lim_{\substack{\Delta\to 0\\ \xi\to 0}} \frac{1}{2}\frac{d^2\xi^2}{d\Delta^2}=0 .$$

It is easy to check that this is the case for Eq. (31), but on the curve of (32)

$$\lim_{\substack{\Delta\to 0\\ \xi\to 0}} \left[\frac{d\xi}{d\Delta}\right]^2 = \lim_{\substack{\Delta\to 0\\ \xi\to 0}} \frac{1}{2}\frac{d^2\xi^2}{d\Delta^2}\to\pm\infty .$$

B. Perturbation of N and θ

This kind of perturbation causes a change in the beamwidth ρ_j, beam amplitude N, and relative beam phase θ. The conditions $\xi=0$ and $\Delta=0$ are maintained in the system, however, so the evolution equations are

$$\frac{dN}{dz}=F\sin\theta , \tag{33}$$

$$\frac{d\theta}{dz}=(1+N)\rho_2-(1-N)\rho_1-\mu\rho_1\rho_2 NA+\frac{\nu}{2}\sqrt{\rho_1\rho_2}\left[\left(\frac{1-N}{1+N}\right)^{1/2}-\left(\frac{1+N}{1-N}\right)^{1/2}\right]B\cos\theta$$
$$-\nu\sqrt{\rho_1\rho_2}\left(\frac{1-N}{1+N}\right)^{1/2}\rho_2\frac{\partial B}{\partial\rho_2}\cos\theta+\nu\sqrt{\rho_1\rho_2}\left(\frac{1+N}{1-N}\right)^{1/2}\rho_1\frac{\partial B}{\partial\rho_1}\cos\theta$$
$$-\frac{\mu}{2}\rho_1\rho_2(1-N)\rho_2\frac{\partial A}{\partial\rho_2}+\frac{\mu}{2}\rho_1\rho_2(1+N)\rho_1\frac{\partial A}{\partial\rho_1}\ , \tag{34}$$

$$\tfrac{2}{3}(1-N-\rho_1)+\nu\left(\frac{1+N}{1-N}\right)^{1/2}\left(\frac{\rho_2}{\rho_1}\right)^{1/2}B\cos\theta+\mu\rho_2(1+N)A$$
$$+2\nu\left(\frac{1+N}{1-N}\right)^{1/2}\sqrt{\rho_1\rho_2}\frac{\partial B}{\partial\rho_1}\cos\theta+\mu\rho_1\rho_2(1+N)\frac{\partial A}{\partial\rho_1}=0\ , \tag{35}$$

$$\tfrac{2}{3}(1+N-\rho_2)+\nu\left(\frac{1-N}{1+N}\right)^{1/2}\left(\frac{\rho_1}{\rho_2}\right)^{1/2}B\cos\theta+\mu\rho_1(1-N)A$$
$$+2\nu\left(\frac{1-N}{1+N}\right)^{1/2}\sqrt{\rho_1\rho_2}\frac{\partial B}{\partial\rho_2}\cos\theta+\mu\rho_1\rho_2(1-N)\frac{\partial A}{\partial\rho_2}=0\ , \tag{36}$$

where

$$A(\rho_1\rho_2)=\int\operatorname{sech}^2(\rho_1 x)\operatorname{sech}^2(\rho_2 x)dx\ ,$$

$$B(\rho_1\rho_2)=\int\operatorname{sech}(\rho_1 x)\operatorname{sech}(\rho_2 x)dx\ ,$$

$$F(N,\rho_1\rho_2)=2\nu\sqrt{1-N^2}\sqrt{\rho_1\rho_2}B\ .$$

Once again, normalized variables have been used.

The system has another constant of motion (the Hamiltonian)

$$E+F\cos\theta=C\ , \tag{37}$$

where the constant $C=\frac{2}{3}(1+\mu)^2+4\nu\cos\theta_0$ is determined from the initial conditions and

$$E(N,\rho_1\rho_2)=\tfrac{2}{3}(1-N)^2\rho_1-\tfrac{1}{3}(1-N)\rho_1^2+\tfrac{2}{3}(1+N)^2\rho_2$$
$$-\tfrac{1}{3}(1+N)\rho_2^2+\mu(1-N^2)\rho_1\rho_2 A\ .$$

Equations (33) and (37) can be developed into

$$\left(\frac{dN}{dz}\right)^2+(C-E)^2-F^2=0\ . \tag{38}$$

The evolution of the system is controlled, therefore, by Eqs. (35)–(38). For any given N, $\rho_{1,2}$ and $\cos\theta$ can be obtained from Eqs. (35)–(37) as a function of N. Consequently, $(C-E)^2-F^2$ is determined as a function of the single variable N, which will be written as $2U(N)$. The initial conditions $\rho_1=\rho_2=1+\mu$, $N|_{z=0}=0$ and $\theta_0=0,\pm\pi$ correspond to $dN/dz|_{z=0}=0$ and $N|_{z=0}=0$, i.e., like a *particle* initially at rest, at the center of a potential well ($N=0$). The stability of the system can then be judged from the character of $d^2U/dN^2|_{N=0}$, i.e., if $d^2U/dN^2|_{N=0}>0$, $N=0$ is a *local minimum* point on the potential curve and the system is stable. On the other hand, if $d^2U/dN^2|_{N=0}<0$, $N=0$ is a *local maximum* and an infinitesimal disturbance will cause the *particle* to roll down a potential hill, with the result that the system is unstable.

The stability edges, after a long calculation, are given by the condition

$$\left.\frac{d^2U}{dN^2}\right|_{N=0}=-4\nu\cos\theta_0\left[\left.\frac{d^2F}{dN^2}\right|_{N=0}\left(\frac{1}{\cos\theta_0}\right)+\left.\frac{d^2E}{dN^2}\right|_{N=0}\right]=0\ , \tag{39}$$

which are

$$\tfrac{8}{3}(1-\mu^2)-\tfrac{8}{3}(1-\mu)\frac{d\rho}{dN}-\frac{4}{1+\mu}(\tfrac{1}{3}+1.21\mu)\left(\frac{d\rho}{dN}\right)^2$$
$$=4\nu\cos\theta_0\left[1+\frac{1.43}{(1+\mu)^2}\left(\frac{d\rho}{dN}\right)^2\right] \tag{40}$$

and

$$\nu\cos\theta_c=0\ , \tag{41}$$

where

$$\frac{d\rho}{dN}=-(1-\mu^2)\Big/\left[1+\frac{4.29\nu\cos\theta_0}{1+\mu}+3.36\mu\right]\ .$$

Equations (40) and (41) are plotted in Fig. 3, together with the result of the linear stability analysis (as modified in this paper) for an asymmetric perturbation. The results show that both TE and TM solitons can be unstable under asymmetric perturbation. Applying the results to different types of nonlinearity gives different $\nu\cos\theta_0$ values for the instability region. In the particular case of a molecular orientational nonlinear mechanism, $\mu\to\infty$. After some manipulation, the present theory predicts that TE solitons, which correspond to $\theta_0=0$, are always stable under an asymmetric perturbation, while TM soli-

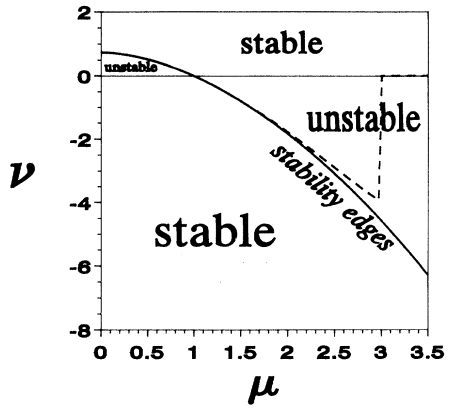

FIG. 3. (ν,μ) plane showing stable and unstable regions for asymmetric perturbations. Solid lines represent the Lagrangian theory and the dashed lined a linear stability analysis.

tons, which correspond to $\theta_0=\pm\pi$, are stable if $\nu\cos\theta_0/\rho^2<1.05$. In the range between $\mu=0$ and 3, the present results are qualitatively similar to the results from linear stability analysis [4].

In the limiting case $\mu=0$ for TE solitons, it has been reported in the literature [6] that instability occurs when $\nu<0.6667$, within a particle theory similar to the one presented here. In this limit, the instability predicted here occurs when $\nu<0.7467$, which is practically the same as the linear stability, which is $\nu<0.75$. Note that Paré and Florjanczyk assumed a constant beamwidth. The TM soliton is always stable for $\mu=0$.

C. Numerical results

For finite μ and ν, it is easy to integrate Eqs. (11) numerically for initial conditions that are close to the stationary, solitary wave solutions given by Eq. (13). Such an integration is reported here to check the predictions of the stability analysis depicted in Figs. 2 and 3. Figures 4 and 5 contain some of the conclusions. The length scale L_z, along the propagation direction, is $L_z=4\pi nD_0^2/\lambda$, where n is the refractive index of the waveguide, λ is the wavelength in a vacuum, and D_0 is the beamwidth. For $\lambda=0.62$ μm, $n=1.53$, and $D_0=8.5$ μm, for example, L_z is 2.24 mm. The numerical work shown in Figs. 4 and 5 agrees very well with the analytical predictions derived in this paper. Numerical experiments that have been reported in the literature [4] also confirm parts of the present theory. An important point to make, however, is that during the course of any numerical simulations, rounding errors will accumulate, so any instability, computationally observed, may be due to this. Indeed, if the propagation is long enough, breakup will be sure to occur. The stability of a system should be judged, therefore, by comparing propagation behavior in the stable and unstable cases over similar distances. The numerical results shown in Figs. 4(a) and 4(b) confirm the stability edge conclusions shown in Fig. 2. Figure 4(a) shows instability setting in at $12L_z$ yet, in Fig. 4(b), even at $24L_z$ no instability is observed. The propagation distance $24L_z$

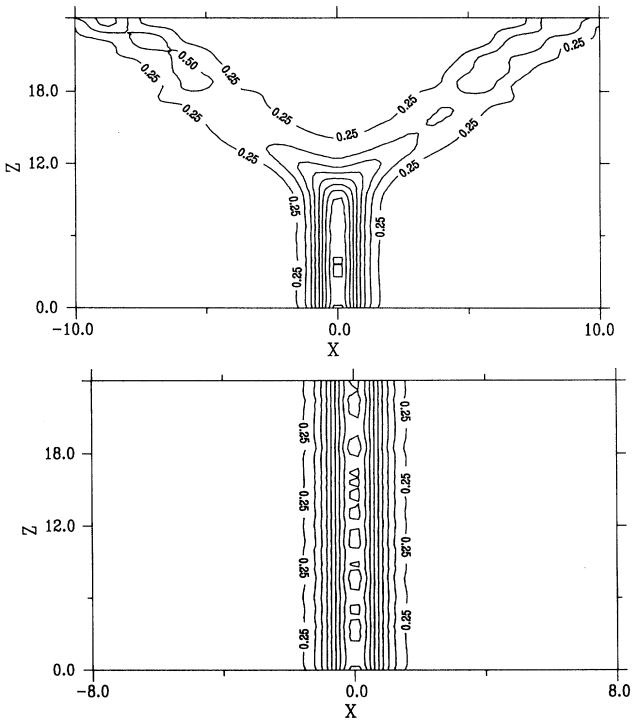

FIG. 4. (a) The contour map of coupled soliton beams over a distance of $z=24L_z$. The x unit is D_0. The coupling coefficients are (a) $\nu=-0.25$ and $\mu=0.2$ and (b) $\nu=-1$ and $\mu=0.2$. The initial perturbation is symmetric with $N=0$, $\Delta=0.01$, and $\xi=0$. z and x are dimensionless.

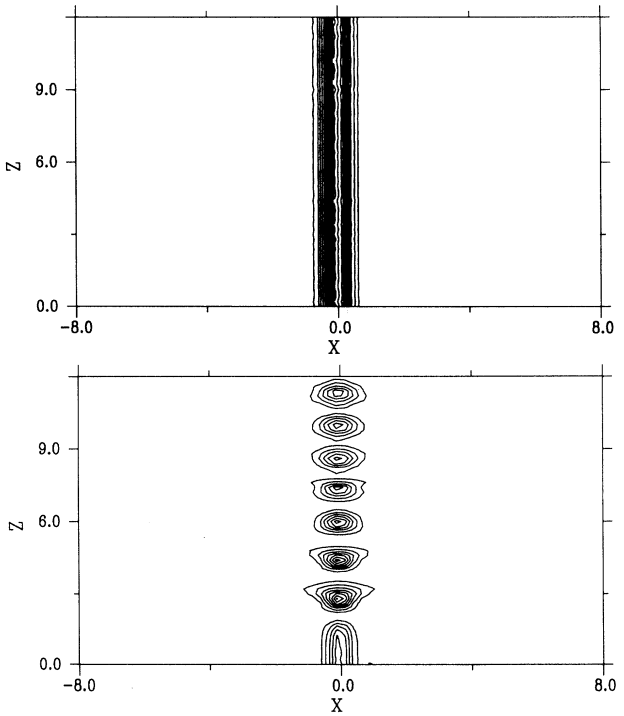

FIG. 5. The contour map of coupled soliton beams over a distance of $z=12L_z$ and $-8D_0\le x\le 8D_0$. The coupling coefficients are (a) $\nu=-3$ and (b) $\nu=-1$ and $\mu=2$. The initial perturbation is asymmetric with $N=0.01$, $\Delta=0$, and $\xi=0$. z and x are dimensionless.

is judged to be long enough for conclusions to be drawn about the physical stability of the system. In fact, Fig. 4(b) breaks up at $z=150L_z$ (because of rounding error), which is more than ten times the breaking distance in Fig. 4(a).

As stated earlier, Fig. 2 shows that the stability edge diagram for symmetry perturbations is quite different from the one obtained by linear stability analysis. In earlier work, the whole region below the dotted line is designated as unstable, whereas the theory reported here concludes that only small portions of this area are unstable. The numerical tests shown in Figs. 4(a) and 4(b) confirm this and every rapidly unstable case in the paper by Wright, Stegeman, and Wabnitz [4] also corresponds to data inside or very close to the unstable regions of Fig. 2. Any previously reported instability in the stable region of Fig. 2 has either been for perturbations that are too large for the perturbation analysis to be valid or for ultralong propagations, by which time the pulse or beam breaks up due to rounding error and should not be interpreted as a physical instability. Figures 5(a) and 5(b) show the numerical confirmations of Fig. 3. In Fig. 5(a) the point $\nu=-3.0,\mu=2.0$ is selected. This point is in the stable region of Fig. 3 and is shown by the simulation to be perfectly stable over a propagation distance of $12L_z$. In Fig. 5(b) the point $\nu=-1.0,\mu=2.0$ of Fig. 3 is selected and is demonstrated to be unstable. Note that the stability regimes in Fig. 3 are very similar to the previously published case. It is emphasized that the mathematical conclusions reached here are borne out by the numerical (exact) simulations, which indicates that good trial functions are being used.

In order to deal with molecular nonlinearity numerically, for which $f=1$ and $\mu\to\infty$, the basic equations should be transformed to

$$
\begin{aligned}
i\frac{\partial\psi_+}{\partial z}+\frac{\partial^2\psi_+}{\partial x^2}+2\nu\psi_-+2(1+f)|\psi_-|^2\psi_+=0\ ,\\
i\frac{\partial\psi_-}{\partial z}+\frac{\partial^2\psi_-}{\partial x^2}+2\nu\psi_++2(1+f)|\psi_+|^2\psi_-=0\ ,
\end{aligned}
\tag{42}
$$

where $\psi_\pm$ are $\psi_+=\psi_1/\sqrt{1-f}$ and $\psi_-=\psi_2/\sqrt{1-f}$ and $\mu=(1+f)/1-f)$.

The numerical results provided in Figs. 6 and 7 for symmetric and asymmetric perturbation, respectively, concern molecular nonlinearity. In the case of in-phase beams (TE solitons), stability is predicted analytically for both symmetric and asymmetric perturbations. In the case of $\pm\pi$ out-of-phase beams (TM solitons), the present theory predicts instability in the ranges (a) $-3/\pi^2>\nu/\rho^2>=\frac{2}{5}$ for symmetric perturbations ($\Delta\neq0$ initially) and (b) $0>\nu/\rho^2>-1.05$ for asymmetric perturbations ($N\neq0$ initially). The numerical results, however, show no dependence on the choice of a specific form of perturbation. In the range $0>\nu/\rho^2>-1.05$, no matter what kind of initial perturbation is used, an asymmetric type of breaking will emerge from the evolutions and the system is unstable. This range covers the symmetric instability range $-3/\pi^2$ to $-\frac{2}{5}$. The system is restabilized after $\nu/\rho^2<-1.05$.

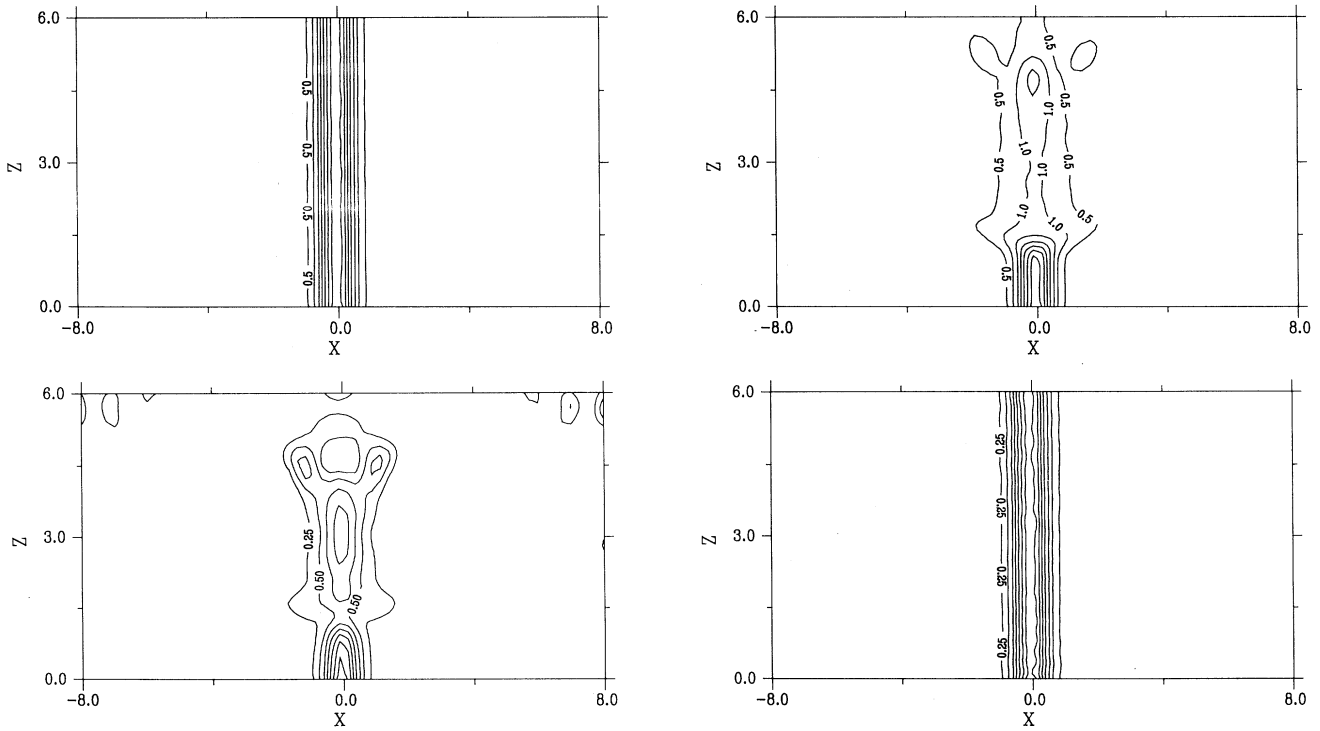

FIG. 6. The contour maps of coupled soliton beams over a distance $z=6L_z$ and $-8D_0\le x\le 8D_0$, in a molecular orientational nonlinear medium. The coupling coefficients are $\nu=0.5,-0.35,-0.6,-1.2$, respectively, for (a)–(d) and the initial perturbation is symmetric. z and x are dimensionless.

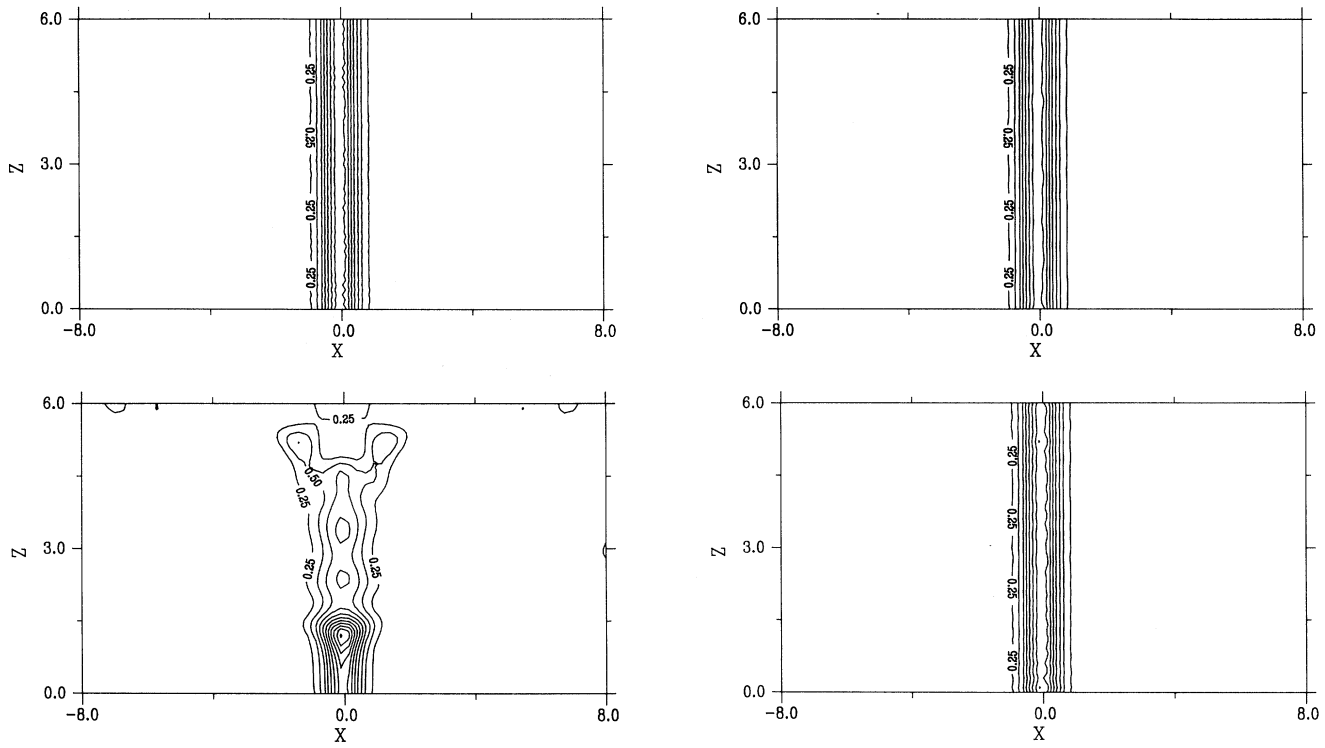

FIG. 7. The contour maps of coupled soliton beams over a distance $z=6L_z$ and $-8D_0 \le x \le 8D_0$, in a molecular orientational nonlinear medium. The coupling coefficients are $\nu=1.5, 0.5, -0.5, -1.5$, respectively, for (a)–(d) and the initial perturbation is asymmetric. z and x are dimensionless.

V. INCLUSION OF A LOCAL PHASE CHANGE RATE (SPATIAL FREQUENCY CHIRP)

The spatial soliton dynamics, described in the preceding sections, will now be extended, with a local phase change across the beam as an additional degree of freedom. This inclusion enables the internal oscillations of the beam to be accounted for. This is achieved by using the more general trial function

$$\psi_j=\eta_j \operatorname{sech}[\rho_j(x-x_j)] \times \exp\left[i\frac{\xi_j}{2}(x-x_j)+i\frac{c_j}{2}(x-x_j)^2+i\theta_j\right], \tag{43}$$

where c_j is a chirp parameter (analogous to the temporal case) and the other parameters have the same meaning as before. Substituting this general trial function into the Lagrangian and then integrating over x yields the averaged Lagrangian

$$\mathcal{L}=\mathcal{L}_1+\mathcal{L}_2+\mathcal{L}_{12}$$

where

$$\mathcal{L}_j=2\left[\frac{\xi_j}{2}\frac{\partial x_j}{\partial z}-\frac{\partial \theta_j}{\partial z}\right]\frac{\eta_j^2}{\rho_j}+\frac{4}{3}\frac{\eta_j^4}{\rho_j}-\frac{2}{3}\rho_j\eta_j^2-\frac{\xi_j^2}{2}\frac{\eta_j^2}{\rho_j}-r\left[c_j^2+\frac{1}{2}\frac{\partial c_j}{\partial z}\right]\frac{\eta_j^2}{\rho_j^3}, \quad j=1,2$$

$$\mathcal{L}_{12}=2\mu\eta_1^2\eta_2^2\int \operatorname{sech}^2[\rho_1(x-x_1)]\operatorname{sech}^2[\rho_2(x-x_2)]dx$$

$$+4\nu\eta_1\eta_2\int \operatorname{sech}[\rho_1(x-x_1)]\operatorname{sech}[\rho_2(x-x_2)] \times\cos\left[\frac{\xi_2}{2}(x-x_2)-\frac{\xi_1}{2}(x-x_1)+\frac{c_2}{2}(x-x_2)^2-\frac{c_1}{2}(x-x_1)^2+\theta_2-\theta_1\right]dx, \tag{44}$$

and $r=\int x^2\,\mathrm{sech}^2 x\,dx$.

The application of the Euler-Lagrange equations then gives the previously reported equations, together with

$$\frac{d}{dz}\left[\frac{\eta_j^2}{\rho_j^3}\right]=4c_j\frac{\eta_j^2}{\rho_j^3}-\frac{2}{r}\frac{\partial L_{12}}{\partial c_j}\ , \tag{45}$$

$$\frac{d\theta_j}{dz}=\eta_j^2+\frac{\xi_j^2}{4}+\frac{2}{3}(\eta_j^2-\rho_j^2)-\frac{1}{2}\frac{\rho_j\xi_j}{\eta_j^2}\frac{\partial L_{12}}{\partial \xi_j}+\frac{1}{4}\frac{\rho_j^2}{\eta_j^2}\frac{\partial L_{12}}{\partial \rho_j}+\frac{3}{8}\frac{\rho_j}{\eta_j}\frac{\partial L_{12}}{\partial \eta_j}\ , \tag{46}$$

$$\frac{d}{dz}(rc_j)=-2rc_j^2-\frac{4}{3}\rho_j^2(\eta_j^2-\rho_j^2)=\frac{\rho_j^4}{\eta_j^2}\frac{\partial L_{12}}{\partial \rho_j}-\frac{1}{2}\frac{\rho_j^3}{\eta_j}\frac{\partial L_{12}}{\partial \eta_j}\ . \tag{47}$$

The stationary solution is

$$x_1=x_2=0,\quad \xi_1=\xi_2=0,\quad c_1=c_2=c=0\ ,$$
$$\rho_1=\rho_2=\rho=(1+\mu)M,\quad \eta_1=\eta_2=\eta=\sqrt{1+\mu}M\ , \tag{48}$$
$$\theta=\theta_2-\theta_1=0,\pm\pi,\quad \frac{d\theta}{dz}=(1+\mu)^2M^2+2\nu\ .$$

This new system of equations still shows that the law of "mass" conservation and "momentum" conservation is satisfied. Also, if a proper coordinate system is used, the "mass center" of the coupled solitons is stationary. Further progress is difficult because of the multicoupling of the variables, even though the variables can be separated into two groups $(\Delta,\xi,\rho_1=\rho_2,c_1=c_2,N=0,\theta=0,\pm\pi)$ and $(\Delta=0,\xi=0,\rho_{1,2},c_{1,2},N,\theta)$. In the following, therefore, the calculations will focus on the special cases $\nu=0$ and $\mu=1$.

A. $\nu=0$

In this case $\eta_j^2/\rho_j=M$ is a constant and

$$\frac{dx_j}{dz}=\xi_j\ , \tag{49}$$

$$\frac{d\xi_j}{dz}=4\mu\eta_k^2\rho_j^2\int \mathrm{sech}^2[\rho_1(x-x_1)]\mathrm{sech}^2[\rho_2(x-x_2)]\tanh[\rho_j(x-x_j)]dx\ , \tag{50}$$

$$\frac{d}{dz}\left[\frac{1}{\rho_j}\right]=\frac{2c_j}{\rho_j}\ , \tag{51}$$

$$\frac{d(rc_j)}{dz}=-2rc_j^2-\tfrac{4}{3}\rho_j^2(\eta_j^2-\rho_j^2)-2\mu\eta_k^2\rho_j^3\int \mathrm{sech}^2[\rho_1(x-x_1)]\mathrm{sech}^2[\rho_2(x-x_2)]dx$$
$$+4\mu\eta_k^2\rho_j^4\int (x-x_j)]\tanh[\rho_j(x-x_j)]\mathrm{sech}^2[\rho_1(x-x_1)]\mathrm{sech}^2[\rho_2(x-x_2)dx \tag{52}$$

where $j,k=1,2$ and $j\neq k$. The Hamiltonian of this system is

$$\sum_{j=1}^{2}\left[-\frac{2}{3}\frac{\eta_j^4}{\rho_j}+\frac{1}{3}\rho_j\eta_j^2+\frac{\xi_j^2}{4}\frac{\eta_j^2}{\rho_j}+\frac{r}{2}\frac{c_j^2\eta_j^2}{\rho_j^3}\right]-\mu\eta_1^2\eta_2^2\int \mathrm{sech}^2[\rho_1(x-x_1)]\times\mathrm{sech}^2[\rho_2(x-x_2)]dx=H\ . \tag{53}$$

1. *Perturbation type A*

If the perturbation is symmetric about ρ_j and c_j, the conditions $\rho_1=\rho_2=\rho$ and $c_1=c_2=c$ are initially satisfied. The system then has the following characteristics: $\xi_2=-\xi_1=\xi$, $x_2=-x_1=\Delta$, $\eta_2=\eta_1=\eta$, $(d/dz)(1/\rho_2-1/\rho_1)=0$, and $(d/dz)(c_2-c_1)=0$. The evolution equations then reduce to

$$\frac{d\Delta}{dz}=\xi,\quad \frac{d}{dz}\left[\frac{1}{\rho}\right]=\frac{2c}{\rho}\ . \tag{54}$$

Consequently, the Hamiltonian of the system is

$$\frac{1}{2}\left[\frac{d\Delta}{dz}\right]^2+\frac{r}{4}\left[\frac{d}{dz}\left[\frac{1}{\rho}\right]\right]^2+\tfrac{2}{3}\rho^2-\tfrac{4}{3}M\rho-\mu M\rho\int \mathrm{sech}^2(x-\rho\Delta)\mathrm{sech}^2(x+\rho\Delta)dx=E\ . \tag{55}$$

Equation (55) can be viewed as the energy conservation law of a particle moving in a two-dimensional potential, with E as the total energy. The position parameters of the particle are $(r_1,r_2)=(\Delta,\sqrt{r/2}(1/\rho))$, time is $t=z$, and the two velocity components are $dr_1/dt=d\Delta/dz$ and $dr_2/dt=\sqrt{r/2}(d/dz)(1/\rho)$.

Hence a two-dimensional potential function exists, which is

$$U(r_1,r_2)=-\frac{4M}{3}\left[\frac{r}{2}\right]^{1/2}\frac{1}{r_2}+\frac{r}{3}\frac{1}{r_2^2}-\mu M\left[\frac{r}{2}\right]^{1/2}\frac{1}{r_2}\int \mathrm{sech}^2\left[x-\left[\frac{r}{2}\right]^{1/2}\frac{r_1}{r_2}\right]\mathrm{sech}^2\left[x+\left[\frac{r}{2}\right]^{1/2}\frac{r_1}{r_2}\right]dx\ . \tag{56}$$

This potential has a minimum value at $r_1=0$ and $r_2=\sqrt{r}/2[1/(1+\mu)M]$, which corresponds to the stationary solution $[\Delta=0,\rho=(1+\mu)M]$ of the system. The second derivatives of U with respect to r_1 and r_2 gives the shape of U at that point so that the stability of the stationary solution can be abstracted. After a lengthy calculation, at the minimum point, the potential satisfies the following conditions:

$$\frac{\partial^2 U}{\partial r_1^2}=\frac{64}{15}\mu M^4(1+\mu)^3 ,$$
$$\frac{\partial^2 U}{\partial r_1 \partial r_2}=0 , \tag{57}$$
$$\frac{\partial^2 U}{\partial r_2^2}=\frac{8}{3r}(1+\mu)^4 M^4 .$$

For a perturbation along a line l, at an angle ϕ to one of the position coordinate directions (r_1, for example),

$$\frac{d^2 U}{dl^2}=\frac{8(1+\mu)^3 M^4}{3[1+\tan^2(\phi)]}\left[\frac{8\mu}{5}+\frac{1+\mu}{r}\tan^2(\phi)\right] , \tag{58}$$

where

$$\tan(\phi)=\frac{\partial r_2}{\partial r_1}=\frac{dr_2/dz}{dr_1/dz}=\sqrt{r}\,\frac{\rho_0-\rho}{\sqrt{2}\Delta\rho\rho_0}=\frac{\sqrt{2r}\,c}{\xi\rho} . \tag{59}$$

Here ξ, ρ, and c are values whose derivations from $\xi_0==0$, $\rho_0=(1+\mu)M$, $c_0=0$, and $\Delta_0=0$ represent the perturbation.

Equation (58) shows that d^2U/dl^2 is always positive, unless $\mu<0$. This shows that the system is stable under this type of perturbation. The perturbation here has the same nature as that in Sec. IV A, since the choice $\nu=0$ corresponds to the μ axis of Fig. 2. The current conclusion confirms part of the previous results, in the presence of chirp.

Using $d^2U/dl^2=0$, gives

$$\mu_1=-1,\quad \mu_2=-k^2/(\frac{16}{5}+k^2) , \tag{60}$$

where

$$k=\left[\frac{2}{r}\right]^{1/2}\tan(\phi)=\frac{\rho_0-\rho}{\Delta\rho\rho_0}=\frac{2c}{\xi\rho} . \tag{61}$$

Figure 8 shows the stability edges predicted by Eqs. (60) and (61). The regions of stability and instability are clearly marked, with two points being selected for numerical simulation tests. The results of these tests are shown in Figs. 9(a) and 9(b). The respective figures show simulations are on ξ and c. The effects are the same if we choose to perturb Δ and ρ from $\Delta_0=0$ and $\rho_0=(1+\mu)M$.

2. *Perturbation type B*

If the perturbation is symmetric about x_j and ξ_j, i.e., the conditions $x_1=x_2=0$ and $\xi_1=\xi_2=0$ are not affected,

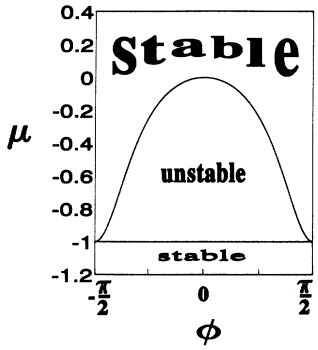

FIG. 8. (μ,ϕ) plane showing stable and unstable regions for solitons, under perturbation type A, that have the form given by Eq. (43).

then the evolution equations reduce to

$$\frac{d}{dz}\left[\frac{1}{\rho_j}\right]=\frac{2c_j}{\rho_j} , \tag{62}$$

$$\frac{d(rc_j)}{dz}=-2rc_j^2-\tfrac{4}{3}\rho_j(\eta_j^2-\rho_j^2)$$
$$-2\mu\eta_k^2\rho_j^3\int \mathrm{sech}^2(\rho_1 x)\mathrm{sech}^2(\rho_2 x)\,dx$$
$$+4\mu\eta_k^2\rho_j^4\int x\tanh(\rho_j x)\mathrm{sech}^2(\rho_1 x)$$
$$\times\mathrm{sech}^2(\rho_2 x)\,dx . \tag{63}$$

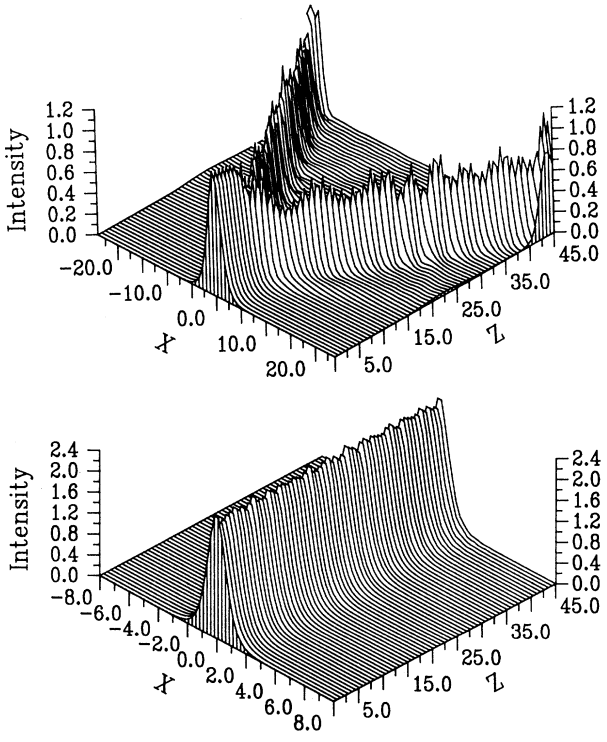

FIG. 9. Surface plots of the coupled solitons over distance $z=45L_z$. The x unit is D_0. The coupling coefficients and initial perturbations are, respectively, (a) $\mu=-0.4$ and $c_1=c_2=0(\phi=0)$ and (b) $\mu=0.2$ and $c_1=c_2=0(\phi=0)$. z and x are dimensionless.

The Hamiltonian can be written, therefore, as

$$E=\frac{3r}{8}\left\{\frac{1}{2}\left[\frac{d}{dz}\left[\frac{1}{\rho_1}\right]\right]^2+\frac{1}{2}\left[\frac{d}{dz}\left[\frac{1}{\rho_2}\right]\right]^2\right\}+\frac{\rho_1^2}{2}+\frac{\rho_2^2}{2}-\rho_1 M-\rho_2 M-\frac{3\mu}{2}\rho_1\rho_2 M\int \operatorname{sech}^2(\rho_1 x)\operatorname{sech}^2(\rho_2 x)\,dx \ . \quad (64)$$

The above equation expresses the energy conservation law, where E is the total energy, $(r_1,r_2)=(1/\rho_1,1/\rho_2)$ is the particle position,

$$\frac{3r}{8}\left\{\frac{1}{2}\left[\frac{d}{dz}\left[\frac{1}{\rho_1}\right]\right]^2+\frac{1}{2}\left[\frac{d}{dz}\left[\frac{1}{\rho_2}\right]\right]^2\right\}$$

is the kinetic energy, and the potential energy

$$U(r_1,r_2)=\frac{1}{2r_1^2}+\frac{1}{2r_2^2}-\frac{M}{r_1}-\frac{M}{r_2}-\frac{3\mu}{2}\frac{M}{r_1 r_2}\int \operatorname{sech}^2\left[\frac{x}{r_1}\right]\operatorname{sech}^2\left[\frac{x}{r_2}\right]dx \ . \quad (65)$$

The minimum point of this potential function is found at $r_1=r_2=1/(1+\mu)M$. After differentiating U twice with respect to r_1 and r_2, it is found, at the minimum point, that

$$\frac{\partial^2 U}{\partial r_1^2}=\frac{\partial^2 U}{\partial r_2^2}=(1+2.31\mu)(1+\mu)^3M^4 \ , \qquad \frac{\partial^2 U}{\partial r_1\partial r_2}=-1.32\mu(1+\mu)^3M^4 \ . \quad (66)$$

Perturbing the system along a line l, at an angle ϕ to r_1, i.e.,

$$k=\tan\phi=\frac{\partial r_2}{\partial r_1}=\frac{dr_2/dz}{dr_1/dz}=\frac{\rho_1(\rho_0-\rho_2)}{\rho_2(\rho_0-\rho_1)}=\frac{c_2\rho_1}{c_1\rho_2} \ ,$$

leads to

$$\frac{d^2U}{dl^2}=\left[1+\left[2.31-\frac{2.64k}{1+k^2}\right]\mu\right](1+\mu)^3M^4 \ . \quad (67)$$

Again this result agrees with Sec. IV that the system is always stable unless $\mu<0$. For the case $\mu<0$, $d^2U/dl^2=0$ gives the stability edges as $\mu_1=-1$, and $\mu_2=-1/[2.31-1.32\sin(2\phi)]$. These solutions are plotted in Fig. 10. Figure 11 shows the stability edges predicted by Eq. (67). The points selected for numerical testing are $\mu=-0.6$ and $\phi=-\pi/4$ (unstable) and $\mu=-0.6$ and $\phi=\pi/4$ (stable). The evolution to instability or stability is displayed in Figs. 11(a) and 11(b).

B. $\mu=1$ with perturbation of η and θ

In this case, $x_1=x_2=0$, $\xi_1=\xi_2=0$, $\rho_1=\rho_2=\rho=(1+\mu)M$, $c_1=c_2=0$, $dx_1/dz=dx_2/dz=0$, $d\xi_1/dz=d\xi_2/dz=0$, $(d/dz)(1/\rho_1)=(d/dz)(1/\rho_2)=0$, and $dc_1/dz=dc_2/dz=0$. The only evolution equations left are

$$\frac{d}{dz}\left[\frac{\eta_j^2}{\rho_j}\right]=-\frac{1}{2}\frac{\partial L_{12}}{\partial\theta_j} \ , \quad (68)$$

$$\frac{d\theta_j}{dz}=\eta_j^2+\frac{1}{4}\frac{\rho_j^2}{\eta_j}\frac{\partial L_{12}}{\partial\rho_j}+\frac{3}{8}\frac{\rho_j}{\eta_j}\frac{\partial L_{12}}{\partial\eta_j} \ . \quad (69)$$

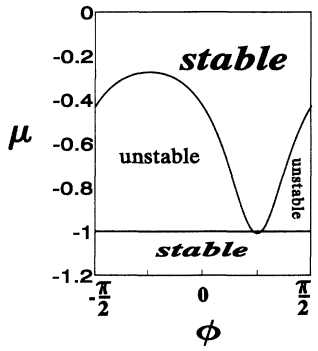

FIG. 10. (μ,ϕ) plane showing stable and unstable regions for chirped solitons, under perturbation type B, that have the form given by Eq. (43).

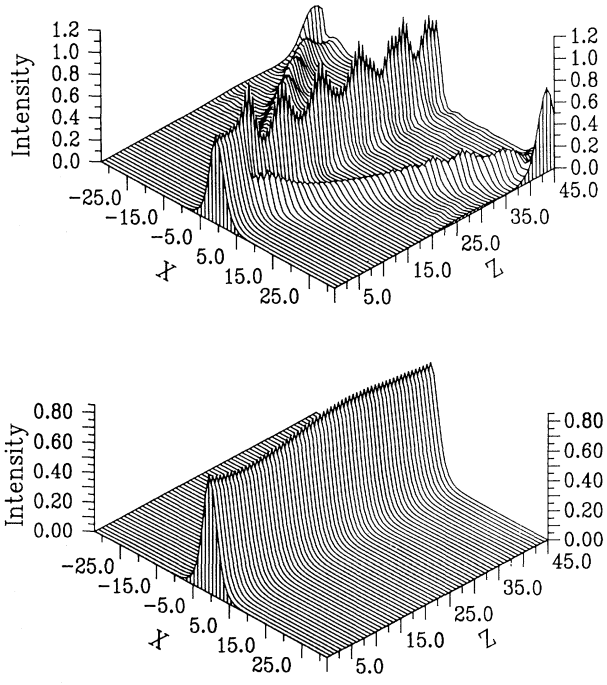

FIG. 11. Surface plots of the coupled solitons over distance $z=45L_z$ and $-32D_0\le x\le 32D_0$. The coupling coefficients and initial perturbations are, respectively, (a) $\mu=-0.6, c_1=0.01$, and $c_2=0.01$, and $c_2=-0.01(\phi=-\pi/4)$ and (b) $c_1=c_2=0.01(\phi=\pi/4)$. z and x are dimensionless.

The Hamiltonian is

$$\frac{1}{3}\frac{\eta_1^4}{\rho_1}+\frac{1}{3}\frac{\eta_2^4}{\rho_2}\frac{1}{6}\rho_1\eta_1^2-\frac{1}{6}\rho_2\eta_2^2+\frac{1}{2}\eta_1^2\eta_2^2\int \operatorname{sech}^4(\rho x)dx + \nu\eta_1\eta_2\int \operatorname{sech}^2(\rho x)dx\cos(\theta_2-\theta_1)=H \ .$$

Defining $\eta_2^2/\rho_2-\eta_1^2/\rho_1=2N$ and using the relations $\frac{\eta_2^2}{\rho_2}+\frac{\eta_1^2}{\rho_1}=2M$ and $\theta_2-\theta_1=\theta$ leads to

$$M\frac{dN}{dz}=4\nu M\sqrt{M^2-N^2}\sin\theta \ , \tag{70}$$

$$H=4\nu M^2\cos\theta_0=4\nu M\sqrt{M^2-N^2}\cos\theta \ , \tag{71}$$

which condenses to

$$\frac{1}{2}\left[\frac{dN}{dz}\right]^2+8\nu^2N^2=0 \ . \tag{72}$$

Obviously, the potential function is $U(N)=8\nu^2N^2$ so that $d^2U/dN^2=16\nu^2$ is always positive, thus indicating that a stable solution is always present. This conclusion confirms the information obtained from Fig. 3, in which the unstable region shrinks to zero at $\mu=1$. Spatial chirp does not change the stability nature of the system.

VI. CONCLUSIONS

This paper contains the results of an investigation of the dynamics of differently polarized spatial solitons in a planar optical waveguide. A full mathematical analysis, obtained via Whitham's variational method, is presented. Analytical results are obtained using comprehensive trial functions, some of which include a local phase change. As in a previous paper [9] the concepts of mass and momentum flow rather easily from this formulation, but the problem addressed concerns the polarization interaction of beams, within the same waveguide. Predictions of stability edges are made and these are supported by numerical simulations of the true soliton dynamics. Both linear ν and nonlinear μ interaction parameters are included in the formalism. No restrictions are placed upon μ and the mathematical work is completely vindicated by the numerical results.

ACKNOWLEDGMENTS

The authors acknowledged support from the United Kingdom Engineering and Physical Sciences Research Council (EPSRC). K.X. is supported by EPSRC.

[1] G. P. Agrawal, *Nonlinear Fiber Optics* (Academic, Boston, 1989).
[2] G. P. Agrawal, J. Opt. Soc. Am. B **7**, 1072 (1990).
[3] C. R. Menyuk, IEEE J. Quantum Electron. **QE-23**, 174 (1987).
[4] E. M. Wright, G. I. Stegeman, and S. Wabnitz, Phys. Rev. A **40**, 4455 (1989).
[5] J. M. Soto-Crespo and N. Akhmediev, Phys. Rev. E **48**, 4710 (1993).
[6] C. Paré and M. Florjanczyk, Phys. Rev. A **41**, 6287 (1990).
[7] V. K. Mesentsev and S. K. Turitsyn, Opt. Lett. **17**, 1497 (1992).
[8] T. Ueda and W. L. Kath, Phys. Rev. A **42**, 563 (1990).
[9] A. D. Boardman and K. Xie, Phys. Rev. A **50**, 1851 (1994).
[10] D. Anderson and M. Lisak, Phys. Rev. A **32**, 2270 (1985).
[11] A. D. Boardman and K. Xie, Radio Sci. **28**, 891 (1993).
[12] F. Reynaud and A. Barthelemy, in *Guided Wave Nonlinear Optics,* Vol. 214 of *NATO Advanced Study Institute, Series E: Applied Science,* edited by D. B. Ostrowky and R. Reinisch (Kluwer, Dordrecht, 1991), p. 319.
[13] J. S. Aitchison, Y. Silberberg, A. M. Weiner, D. E. Laird, M. K. Oliver, J. L. Jackel, E. M. Vogel, and P. W. E. Smith, J. Opt. Soc. Am. B **8**, 1290 (1991).
[14] J. S. Aitchison, K. Al-Hemyani, C. N. Ironside, R. S. Grant, and W. Sibbett, Electron. Lett. **28**, 1879 (1992).
[15] A. Barthelemy, S. Manuef, and F. Froehly, Opt. Commun. **55**, 201 (1985).
[16] R. de la Fuente and A. Barthelemy, Opt. Commun. **88**, 419 (1992).
[17] S. A. Akhmanov, A. P. Sukhorukov, and R. V. Khokhlov, Usp. Fiz. Nauk **93**, 19 (1967) [Sov. Phys. USP. **93**, 609 (1968)].
[18] D. J. Kaup, B. A. Malomed, and R. S. Tasgal, Phys. Rev. E **48**, 3049 (1993).
[19] B. A. Malomed, Phys. Rev. A **43**, 410 (1991).
[20] T. Ueda and W. L. Kath, Physica D **55**, 166 (1992).
[21] Y. S. Kivshar, J. Opt. Soc. Am. B **7**, 2204 (1990).
[22] D. Anderson, M. Lisak, and T. Reichel, J. Opt. Soc. Am. B **5**, 207 (1988).
[23] G. B. Whitham, *Linear and Nonlinear Waves* (Interscience, New York, 1973).
[24] A. D. Boardman, P. Egan, T. Twardowski, and M. Wilkins, in *Nonlinear Waves in Solid State Physics,* Vol. 247 of *NATO Advanced Study Institute, Series B: Physics,* edited by A. D. Boardman *et al.* (Plenum, New York, 1990).
[25] A. D. Boardman, P. Egan, F. Lederer, U. Langbein, and D. Mihalache, in *Nonlinear Surface Electromagnetic Phenomena,* edited by H. E. Ponath and G. I. Stegeman (Elsevier Science, Amsterdam, 1991).
[26] P. M. Morse and H. Fesbach, *Methods of Theoretial Physics* (McGraw-Hill, New York, 1953).